SCIENCE CHINA
Information Sciences

• MOOP •

February 2020, Vol. 63 124202:1–124202:3
https://doi.org/10.1007/s11432-018-9795-y

Thrust vectoring control of vertical/short takeoff and landing aircraft

Xiangyang WANG[1], Bin ZHU[2], Jihong ZHU[1*] & Zhiqiang CHENG[1]

[1]*Department of Computer Science and Technology, Tsinghua University, Beijing* 100084*, China;*
[2]*Automation Academy, Nanjing University of Science and Technology, Nanjing* 210094*, China*

Received 6 November 2018/Accepted 18 February 2019/Published online 16 January 2020

Citation Wang X Y, Zhu B, Zhu J H, et al. Thrust vectoring control of vertical/short takeoff and landing aircraft. Sci China Inf Sci, 2020, 63(2): 124202, https://doi.org/10.1007/s11432-018-9795-y

Thrust-vectored vertical and/or short take-off and landing (V/STOL) aircraft use a vertical lift fan and a 3-bearing swivel duct (3BSD) nozzle to deliver vertical takeoff, landing and short take-off capability. The bandwidth and efficiency of thrust vectoring effectors are different from that of conventional aerodynamic actuators [1]. Moreover, these effectors have to work near their position/rate limits to take off and land as fast as possible.

The feedback linearization (FBL) control method with control allocation module has been investigated and applied to X-35B aircraft [2]. Ref. [3] studied the optimal trajectory transition controller for V/STOL aircraft. However, few studies have considered the dynamics of the thrust vectoring system. Additionally, chattering problem of effectors has been reported for the X-35B aircraft [2].

This study aims to build a dynamic model for a scaled V/STOL aircraft, namely THU-F35B. A control scheme comprising of the dynamic characteristics of the thrust vectoring system was developed for V/STOL aircraft. Simulation and experimental results are presented.

Dynamic model of the thrust vectoring system. The THU-F35B, as shown in Figure 1(a), is a 1/9 scale of the F-35B fighter developed by Tsinghua University. Its thrust vectoring system includes the main engine, a 3BSD nozzle and a lift fan.

A dynamic model for the main engine has been developed previously [4]. Thrust is a cubic polynomial function of the rotor speed (Ω). The transient dynamics of the fuel flow to the rotor speed is approximated by linear first-order dynamics with a time delay. A similar model was built for the lift fan. Figure 1(b) illustrates the components of the 3BSD nozzle. 3BSD nozzle deflects more than 90 degrees through rotations of three revolute pairs in transition flights of V/STOL aircraft. The nonlinear relation between the deflection angle/direction and the rotation angles is written as [5]

$$\begin{cases} \delta_{\text{N\_angle}} = 2\arccos(\sin^2\zeta\cos\omega_2 + \cos^2\zeta), \\ \delta_{\text{N}y} = \omega_1 + \arctan(\tan(\omega_2/2)\cos\zeta), \end{cases} \tag{1}$$

where ζ denotes the inclination angle of the ducts, ω_1 denotes the rotation angle of the first revolute pair, and ω_2 denotes that of the second and third revolute pairs. Parameters for the 3BSD nozzle of the THU-F35B include: $\zeta = 25^\text{o}$, $\omega_1 \in [-105^\text{o}, 0]$, $\omega_2 \in [0, 180^\text{o}]$, $\delta_{\text{N\_angle}} \in [0, 100^\text{o}]$ (denotes the deflection angle of the nozzle), and $\delta_{\text{N}y} \in [-15^\text{o}, 15^\text{o}]$ (denotes the deflection direction angle) [5].

The vectoring system was installed on a six-component balance. Both static and dynamic experiments were performed and the vectoring force was recorded. The thrust loss increased with an increase in the deflection angle of the nozzle. This relation is described by a second order function:

$$\eta = \eta_0 + \eta_1\delta^2_{\text{N\_angle}}, \tag{2}$$

where η_0 and η_1 are parameters derived by fitting

* Corresponding author (email: jhzhu@tsinghua.edu.cn)

the polynomial function to the static test data. The internal airflow deflects twice in the 3BSD nozzle at each deflection angle up to approximately 50 degrees. The deflection angle of vectored force is inconsistent with the geometric deflection angle. Their relation is modeled as

$$\delta_{\mathrm{N\_force}} = p_1 \delta_{\mathrm{N}}, \tag{3}$$

where p_1 is a parameter derived by fitting this function to the static test data. Flow separation occurs at a large deflection angle and results in significant hysteresis characteristics for the vectored force. The hysteresis characteristics vary with the deflection angle of the nozzle. Herein, a discrete first-order equation was applied to model the relation between the force deflection angle and geometric deflection angle:

$$\delta_{\mathrm{N}}(k) = a\delta_{\mathrm{N}}(k-1) + (1-a)\delta_{\mathrm{N\_angle}}, \tag{4}$$

where $a \in (0,1)$. Components of the vectored forces in the body axis are written as

$$\begin{cases} T_{\mathrm{N}x} = T_{\mathrm{e}}\eta\cos\delta_{\mathrm{N\_force}}, \\ T_{\mathrm{N}y} = T_{\mathrm{e}}\eta\sin\delta_{\mathrm{N\_force}}\sin\delta_{\mathrm{N}y}, \\ T_{\mathrm{N}z} = -T_{\mathrm{e}}\eta\sin\delta_{\mathrm{N\_force}}\cos\delta_{\mathrm{N}y}, \end{cases} \tag{5}$$

where $T_{\mathrm{e}} = f(\Omega)$ is the thrust generated by the main engine in combination with the position and rate saturations of ω_1, ω_2, and Ω to construct the dynamic model of the thrust vectoring system.

Dynamic model of V/STOL aircraft. The aerodynamic forces of a V/STOL aircraft include both the power-off aerodynamic forces/moments and the forces induced by the propulsion system. By translating the vectored forces and aerodynamic forces into the earth-fixed reference frame, the longitudinal dynamic model of V/STOL aircraft can be stated as

$$\begin{cases} \dot{V}_{xg} = (F_{axg} + F_{Txg})/m, \\ \dot{V}_{zg} = (F_{azg} + F_{Tzg})/m + g, \\ \dot{q} = (M_{ay} + M_{Ty})/I_{yy}, \\ \dot{\theta} = q, \end{cases} \tag{6}$$

where F_{Txg} and F_{Tzg} denote the components of the vectored force and F_{axg} and F_{azg} denote components of the aerodynamic force. By including (2), (3), and (5) into the above equation, the dynamic model for V/STOL aircraft can be rewritten as follows:

$$\begin{cases} \dot{\boldsymbol{x}} = \boldsymbol{f}(\boldsymbol{x}) + \boldsymbol{g}(\boldsymbol{x},\boldsymbol{u}) + \boldsymbol{D}\boldsymbol{d}, \\ \boldsymbol{y} = \boldsymbol{C}\boldsymbol{x}, \\ \boldsymbol{u}_{\min} \leqslant \boldsymbol{u} \leqslant \boldsymbol{u}_{\max}, \\ |\dot{\boldsymbol{u}}| \leqslant \boldsymbol{u}_{\mathrm{ratmax}}(\delta_{\mathrm{N\_angle}}), \end{cases} \tag{7}$$

where $\boldsymbol{x} = [V_{xg}\ V_{zg}\ q\ \theta]^{\mathrm{T}}$, $\boldsymbol{u} = [\delta_e\ T_F\ \Omega\ \delta_{\mathrm{N}}]^{\mathrm{T}}$, $\boldsymbol{D} = \mathrm{diag}\{\boldsymbol{I}_3, \boldsymbol{0}\}$, $\boldsymbol{f}(\boldsymbol{x}) = [f_1(\boldsymbol{x})\ \cdots\ f_4(\boldsymbol{x})]^{\mathrm{T}}$ and $\boldsymbol{g}(\boldsymbol{x}) = [g_1(\boldsymbol{x})\ \cdots\ g_4(\boldsymbol{x})]^{\mathrm{T}}$ denote the nonlinear aerodynamic forces and forces/moments of the effectors. The disturbance vector $\boldsymbol{d} = [d_1\ d_2\ d_3]^{\mathrm{T}}$ is included to model the mismatches between the plant and nominal model as well as external disturbances acting on the plant.

Flight control scheme. The dynamic system represented by the above equation is a highly cross-coupled system. The bandwidth of the thrust vectoring system is much lower than that of the aerodynamic actuators. The model predictive control (MPC) algorithm can systematically handle nonlinear MIMO system dynamics while considering the constraints on actuated and controlled signals [6]. This study proposes a modified linear time-varying (LTV) MPC control scheme, as shown in Figure 1(c). The controller was designed based on an extended system that is a combination of the locally linearized system dynamic model of V/STOL aircraft and the dynamic model of the thrust vectoring system.

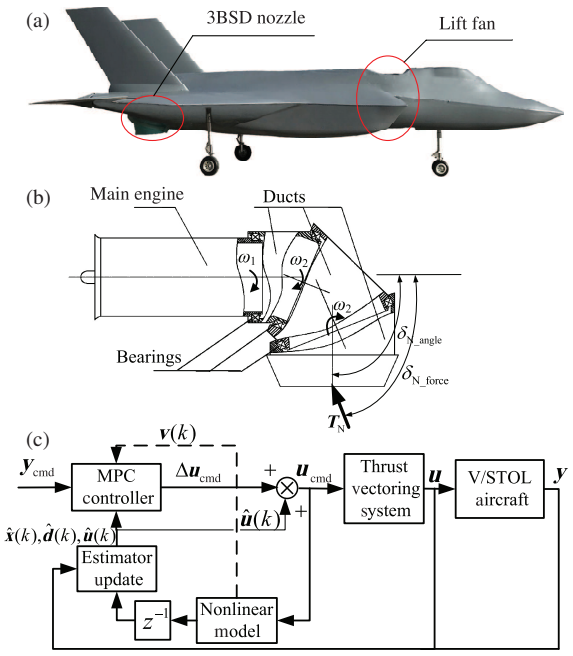

Figure 1 (Color online) THU-F35B, 3BSD nozzle and flight control structure. (a) The THU-F35B aircraft; (b) 3BSD nozzle with deflection angle of 90 degrees; (c) structure of the LTV MPC controller.

Assumption 1. f_i and h_i are assumed to be continuously differentiable on $\boldsymbol{x}$. g_i values are continuous functions of $\boldsymbol{x}$. It is assumed that the Jacobian matrices of $\partial \boldsymbol{f}/\partial \boldsymbol{x}$, $\partial \boldsymbol{g}/\partial \boldsymbol{x}$, $\partial \boldsymbol{g}/\partial \boldsymbol{u}$, and $\partial \boldsymbol{h}/\partial \boldsymbol{x}$ are bounded continuous functions.

The nonlinear system (7) is locally linearized at arbitrary (non-equilibrium) operating points, which are denoted by $(\hat{\boldsymbol{x}}, \hat{\boldsymbol{u}})$. The LTV approximation of the nonlinear system is written as

$$\begin{cases} \dot{\boldsymbol{x}} = \boldsymbol{A}_k\boldsymbol{x} + \boldsymbol{B}_k\boldsymbol{u} + \boldsymbol{v}_k + \boldsymbol{D}\boldsymbol{d}^*, \\ \boldsymbol{y} = \boldsymbol{x}, \end{cases} \tag{8}$$

where $\boldsymbol{A}_k = \partial\boldsymbol{f}/\partial\boldsymbol{x} + \partial\boldsymbol{g}/\partial\boldsymbol{x}|_{\boldsymbol{x}=\hat{\boldsymbol{x}},\boldsymbol{u}=\hat{\boldsymbol{u}}}$, $\boldsymbol{B}_k = \partial\boldsymbol{g}/\partial\boldsymbol{u}|_{\boldsymbol{x}=\hat{\boldsymbol{x}},\boldsymbol{u}=\hat{\boldsymbol{u}}}$, $\boldsymbol{v}_k = \boldsymbol{f}(\hat{\boldsymbol{x}}) + \boldsymbol{g}(\hat{\boldsymbol{x}},\hat{\boldsymbol{u}}) - \boldsymbol{A}_k\hat{\boldsymbol{x}} - \boldsymbol{B}_k\hat{\boldsymbol{u}}$ is the measured disturbance and can be calculated prior to the MPC optimization, $\boldsymbol{d}^*$ is the modified disturbance vector that includes both modeling mismatches and the linearized error. Combining (8) with discretized (4) and the nonlinear equation of T_e, the extended dynamic system can be derived as follows:

$$\begin{cases} \boldsymbol{x}_1(k+1) = \boldsymbol{F}_k\boldsymbol{x}_1(k) + \boldsymbol{G}\boldsymbol{u}_{\mathrm{cmd}}(k) \\ \qquad\qquad + \boldsymbol{\Gamma}\boldsymbol{v}(k) + \boldsymbol{\Phi}\boldsymbol{d}^*(k), \\ \boldsymbol{y}(k) = \boldsymbol{C}\boldsymbol{x}_1(k), \\ \underline{\boldsymbol{u}} \leqslant \boldsymbol{u}_{\mathrm{cmd}}(k) \leqslant \overline{\boldsymbol{u}}, \\ |\Delta\boldsymbol{u}_{\mathrm{cmd}}(k)| \leqslant T_s\boldsymbol{u}_{\mathrm{ratmax}}, \end{cases} \tag{9}$$

where $\boldsymbol{x}_1 = [\boldsymbol{x}\ \Omega\ \delta_{\mathrm{N}}]^{\mathrm{T}}$, $\boldsymbol{u}_{\mathrm{cmd}} = [\delta_e\ T_F\ \Omega_{\mathrm{input}}\ \omega_2]^{\mathrm{T}}$, and $\boldsymbol{F}_k$, $\boldsymbol{G}$, $\boldsymbol{\Gamma}$ and $\boldsymbol{\Phi}$ can be obtained from (4), (8) and the sampling time ΔT. This extended dynamic model is detectable in jet-born flight. An extended Kalman filter was designed to predict the estimated state $\hat{\boldsymbol{x}}_1$ and disturbance $\hat{\boldsymbol{d}}^*$.

This control scheme was designed based on the dynamic model described in (9). The performance index to be minimized is the sum of quadratic terms over the prediction horizon, which is formulated as

$$\begin{aligned} J = &\sum_{i=1}^{H_p} \|\boldsymbol{Q}_x\left[\boldsymbol{x}_1(k+i) - \boldsymbol{x}_{1,\mathrm{ref}}(k)\right]\|_2 \\ &+ \sum_{i=1}^{H_c} \|\boldsymbol{R}_v\Delta\boldsymbol{u}(k+i)\|_2, \end{aligned} \tag{10}$$

where $\boldsymbol{x}_{1,\mathrm{ref}}(k) = [\boldsymbol{x}_{\mathrm{ref}}(k), \boldsymbol{u}_{\mathrm{des}}(k)]^{\mathrm{T}}$ is the desired state of the aircraft and the effectors, and $\boldsymbol{Q}_x$ and $\boldsymbol{R}_v$ are weighting matrices. $\Delta\boldsymbol{u}(k+i)$ is calculated by solving the optimization problem described in the above equation.

Herein, we designed a robust control strategy based on transit for V/STOL aircraft from hover to level flight. A reference state guaranteeing that the aerodynamic lift is larger than the gravity force was calculated firstly. Preferred values of the thrust vectoring system were formulated as functions of the airspeed. Optimization of the MPC controller guarantees that both the states and the effectors are near their desired values. The flight transition is made when the thrust vectoring system satisfies a predefined constraint. This control strategy can achieve smooth autonomous transitions in the presence of modeling errors.

Simulation and experimental results. The proposed controller and FBL controller combined with a piecewise linear mixed optimization control allocation module were designed and simulated. The jet-induced forces/moments were included in the dynamic simulation module, while the dynamic model used for the controllers design assumes that these forces/moments were unknown. Simulation results showed the aircraft with a FBL controller required approximately 25 s to transit from jet-born to wing-born flight. The height and pitch angle of the aircraft oscillate during transition. For the proposed controller, the transition was found to be smooth and was completed in 13 s. The THU-F35B was tested and it achieved successful vertical takeoff, landing, and low-speed forward flights.

Conclusion. The test results of the thrust vectoring system show that V/STOL aircraft are nonlinear overactuated systems with low-bandwidth effectors. A dynamic model of V/STOL aircraft including dynamic characteristics of the thrust vectoring system is proposed. The proposed LTV MPC controller was designed based on the locally linearized model of the aircraft and thrust vectoring system. Simulation and experimental results show that the controller is robust to modeling errors and can achieve tight and fast control over numerous limits through integrated optimization.

Acknowledgements This work was supported by National Natural Science Foundation of China (Grant Nos. 61603210, 61673240) and Aeronautical Science Foundation of China (Grant No. 20160758001).

Supporting information Videos and other supplemental documents. The supporting information is available online at info.scichina.com and link.springer.com. The supporting materials are published as submitted, without typesetting or editing. The responsibility for scientific accuracy and content remains entirely with the authors.

References

1 Walker G P, Wurth S, Fuller J. F-35B integrated flight-propulsion control development. In: Proceedings of International Powered Lift Conference, Los Angeles, 2013
2 Gregory P W, David A A. X-35B STOVL flight control law design and flying qualities. In: Proceedings of Biennial International Powered Lift Conference and Exhibit, Williamsburg, 2002
3 Cheng Z Q, Zhu J H, Yuan X M, et al. Design of optimal trajectory transition controller for thrust-vectored V/STOL aircraft. Sci China Inf Sci, 2018. doi: 10.1007/s11432-018-9582-6
4 Yang J L, Zhu J H. Dynamic modelling of a small scale turbojet engine. In: Proceedings of European Control Conference, Linz, 2015. 2750–2755
5 Wang X Y, Zhu J H, Yang J L, et al. Coordination control strategy based on characteristic model for 3-bearing swivel duct nozzles. Sci China Technol Sci, 2014, 57: 2347–2356
6 Albin T. Benefits of model predictive control for gasoline airpath control. Sci China Inf Sci, 2018, 61: 070204